International Journal of Multiphase Flow 36 (2010) 93–99

Contents lists available at ScienceDirect

International Journal of Multiphase Flow

journal homepage: www.elsevier.com/locate/ijmulflow

Review

A review of research on cylindrical particulate flows

Jianzhong Lin *, Xiaoyu Liang

China Jiliang University, Hangzhou 310018, China
State Key Laboratory of Fluid Power Transmission and Control, Zhejiang University, Hangzhou 310027, China

ARTICLE INFO

Article history:
Received 9 October 2008
Received in revised form 7 May 2009
Accepted 8 May 2009
Available online 18 May 2009

Keywords:
Cylindrical particulate flow
Motion
Sedimentation
Rheology
Hydrodynamic instability
Review

ABSTRACT

The study of cylindrical particulate flows has wide industrial applicability hence received much attention. The purpose of the present paper is to provide a review on our research over the last few years. The research is related to the motion of cylindrical particles in mixing layer, pipe flow, channel flow, converging channel flow; the sedimentation of cylindrical particles in a Newtonian fluid; the structural feature and rheological property of cylindrical particulate suspensions; and the hydrodynamic instability of cylindrical particulate suspensions.

© 2009 Elsevier Ltd. All rights reserved.

1. Introduction

Suspensions of cylindrical particles in either Newtonian or non-Newtonian fluids are often encountered in the physical, engineering and biological sciences. For example, the manufacture of particle-laden products such as reinforced composites, paints, paper, slurries, cements etc. involves the processing of particle suspensions. Drag reduction in flows, affected by suspending a very small concentration of cylindrical particles, is another application. The characterization of the flow or the cylindrical particle orientation in a suspension is of particular interest in the industrial processing research. When particles form a flow-induced orientation state, particle suspension exhibits anisotropy. Therefore, the addition of cylindrical particles to a Newtonian fluid can drastically change the flow kinematics even at very low concentrations, and the importance of coupling flow field and particle orientation has been recognized. Besides, the flow can induce a preferred orientation of the particles which, upon solidification, influences the mechanical properties of the resulting particle-reinforced composite. The composite is stiffer and stronger in the direction of greatest orientation, and weaker and more compliant in the direction of least orientation.

The most common method of studying cylindrical particle motion in flow is the Lagrangian approach, where the trajectory of individual particles is determined by integrating the equations of motion through a known fluid velocity field. The other method is an Eulerian continuum approach. There are two continuum approaches in the theory of two-phase flow, the one-fluid model and the two-fluid model. The former treats the suspension as a single medium whose properties, such as viscosity, are modified in order to account for the presence of suspended matter. A single set of conservation equations, which applies to the bulk suspension, is used. Two-fluid models treat the suspension as two interacting continua, each component phase having its own properties like velocity and concentration, and having its own set of continuum equations. The two-fluid approach is more appropriate than the one-fluid approach in situations where there is a significant slip velocity between the two phases, or when the properties of the particles such as velocity, concentration and configuration are of interest. In the case of cylindrical particulate suspension, slip between the carrier fluid and suspended particles may be caused by particle inertia, by a mismatch between particle injection velocity and carrier fluid velocity, by the internal stress in the particles, by unequal densities of the two phases, by particle–particle interaction, or possibly by different wall boundary conditions for the particulate and carrier fluid phases. In this review, the Lagrangian approach and the one-fluid model of continuum approach are reviewed.

Over the past five years, the cylindrical particulate suspensions have received much attention. A brief review on our research is presented in the following. The cylindrical particles concerned with in this review are straight, stiff and non-Brownian. Besides, the two-fluid model is not covered here.

* Corresponding author. Address: State Key Laboratory of Fluid Power Transmission and Control, Zhejiang University, Hangzhou 310027, China. Tel.: +86 571 86836009; fax: +86 571 87951464.
E-mail address: mecjzlin@public.zju.edu.cn (J. Lin).

0301-9322/$ - see front matter © 2009 Elsevier Ltd. All rights reserved.
doi:10.1016/j.ijmultiphaseflow.2009.05.004

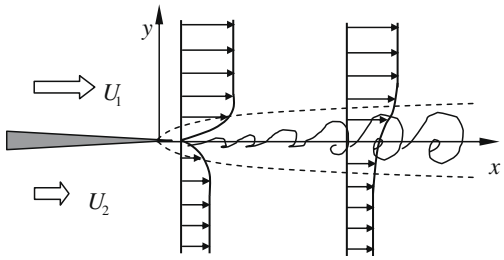

Fig. 1. Schematics of mixing layer.

2. Several typical cylindrical particulate flows

2.1. Mixing layer

The mixing layer, as shown in Fig. 1, represents a typical shear flow and thus provides a building block for many practical inhomogeneous flows such as wakes and jets. In engineering applications, the particle dispersion in mixing layers is of importance, for example, a coal-fired power plant relies on the proper dispersion of particles in the feed jets to provide a well-mixed gas-particle flow for efficient combustion. The proper design of the flow processes depends heavily on the understanding of the dispersion of particles. The mixing layer is a typical flow which involves large-scale vortex. The traditional approach of dealing with the dispersion of particles is to regard the process as Fickian diffusion process and to quantify the mass transfer of particulates with a diffusion coefficient and a particle concentration gradient. This model may be adequate for near-isotropic turbulent flows, however, is not suited to the anisotropic turbulent flows with large vortex structure such as an evolving mixing layer. Therefore, the behavior of cylindrical particles in an evolving mixing layer is investigated numerically with one-way coupling method (Lin et al., 2003a).

The momentum equation of fluid is:

$$\frac{\partial \boldsymbol{u}}{\partial t}+\boldsymbol{\omega}\times\boldsymbol{u}=-\nabla P+\frac{1}{Re}\nabla^2\boldsymbol{u}, \tag{1}$$

where u is the velocity, $\boldsymbol{\omega}=\nabla\times\boldsymbol{u}$ is the vorticity, $P=p+|\boldsymbol{u}|^2/2$is the total pressure, Re is the Reynolds number, $Re=(U_1-U_2)\theta_0/\nu$ (θ_0; is the momentum thickness of the mixing layer, ν is the viscosity, U_1 and U_2 are shown in Fig. 1).

The flow around each particle is considered as the Stokes flow. The size of each particle is much smaller than the scale of the flow field. The interactions between particles are neglected. The slender-body theory (Batchelor, 1970) is used to represent the disturbance velocity created by a particle as an integral of Stokeslets distributed along the particle axis. Then the motion of the particles satisfies the following equation (Mackaplow and Shaqfeh, 1998):

$$\begin{aligned}&\boldsymbol{U}+(\boldsymbol{\Omega}\times s\boldsymbol{p})-\boldsymbol{u}^{\infty}(\boldsymbol{x}_c+s\boldsymbol{p})\\&=-2\left(\ln 2\beta+\ln\frac{\sqrt{1-s^2}}{b(s)}\right)(\boldsymbol{\delta}+\boldsymbol{pp})\cdot\boldsymbol{f}(s)\\&\quad-(\boldsymbol{\delta}-3\boldsymbol{pp})\cdot\boldsymbol{f}(s)-(\boldsymbol{\delta}+\boldsymbol{pp})\cdot\int\frac{\boldsymbol{f}(s)-\boldsymbol{f}(s')}{|s-s'|}\mathrm{d}s'\end{aligned} \tag{2}$$

where $\boldsymbol{U}$ and $\boldsymbol{\Omega}$ are the translational and angular velocity of the particle, $\boldsymbol{p}$ is the orientation unit vector of a particle, s is the distance from the center of the particle, $\boldsymbol{u}^{\infty}$ is the undisturbed fluid velocity, $\boldsymbol{x}_c$ is the particle center position, $\boldsymbol{\beta}$ is the particle aspect ratio, $\boldsymbol{b}$, a shape factor, equals unity for cylindrical particle, and $f(s)$ is the density distribution of the force along the axis of a particle. The integral in Eq. (2) is evaluated by 11-point Gauss–Legendre integration, and then $f(s)$ is obtained by solving the resulting linear equations. The force and torque on a particle are:

$$\boldsymbol{F}=8\pi\mu l\int_{-1}^{1}\boldsymbol{f}(s)\mathrm{d}s,\quad \boldsymbol{T}=8\pi\mu l^2\int_{-1}^{1}s\boldsymbol{p}\times\boldsymbol{f}\mathrm{d}s \tag{3}$$

where μ is the fluid viscosity, l is the half length of particle. The particle's motion is obtained by solving the equation:

$$\frac{d\boldsymbol{u}_p}{dt}=\frac{1}{St}\int_{-1}^{1}\boldsymbol{f}(s)ds, \tag{4}$$

$$\frac{d\Omega_x}{\mathrm{d}t}=\frac{3}{St\beta}\left(\frac{4St}{Re\rho^*}\right)^{-\frac{1}{2}}T_x+\Omega_y\Omega_z,\ \frac{\mathrm{d}\Omega_y}{dt}=\frac{3}{St\beta}\left(\frac{4St}{Re\rho^*}\right)^{-\frac{1}{2}}T_y-\Omega_z\Omega_x,$$

$$\frac{d\Omega_z}{dt}=\frac{2\beta}{St}\left(\frac{4St}{Re\rho^*}\right)^{-\frac{1}{2}}T_z \tag{5}$$

where $\boldsymbol{u}_p$ is the particle velocity, Stokes number is defined as $St=\rho_p a^2\Delta U/4\mu\theta_0$ (ρ_p is the particle density, a is the particle radius, ΔU isU_1-U_2), ρ^* is the particle-to-fluid density ratio, Ω_x, Ω_y and Ω_z are the components of particle angular velocity, T_x, T_y, and T_z are the components of torque.

The equation for the fluid is solved by the spectral method. The effects of St number, particle-to-fluid density ratio ρ^* and particle aspect ratio β on the spatial and orientation distributions of particles are examined. In the computation, we have $0.01\leqslant St\leqslant 1$, $1\leqslant\rho^*\leqslant 775$ and $15\leqslant\beta\leqslant 50$. The results showed that the St number is the key parameter in determining the spatial distribution of particles in the vortex structures, but its effect on the orientation distribution of particles is insignificant. The orientation distribution of particles is controlled mainly by the large vortex structure, for example, as shown in Fig. 2. Both particle-to-fluid density ratio and particle aspect ratio have marginal effects on the spatial and orientation distributions of particles.

2.2. Pipe flow

Cylindrical particulate pipe flow, as shown in Fig. 3, can be found in many areas of industry, such as the production of composite materials, environmental engineering, chemical engineering, pneumatic conveying and so on. The earlier works were concerned with the relationship between the orientation distribution of particles and Re number. The effects of shear rate of flow, particle aspect ratio and particle density on the orientation distribution of particles, however, appears to be an unexplored topic of research. Lin et al. (2004a) simulated numerically the spatial and orientational distributions of cylindrical particles in laminar and turbulent pipe flows with one-way coupling method. The assumptions about the particles are same as those mentioned above. The motion of the particles is simulated numerically based on Eqs. (2)–(5). In order

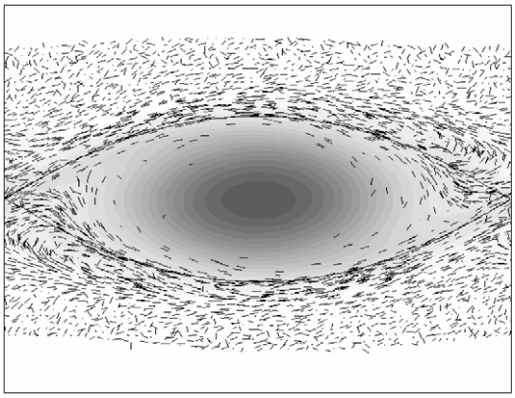

Fig. 2. Distributions of particles for $St=0.1$, $Re=400$, $\beta=30$, $\rho^*=755$ at $T=10$.

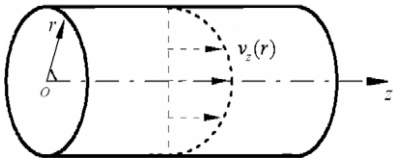

Fig. 3. Schematics of pipe flow.

to simulate the motion of particles, the flow field should be known priori. For a laminar pipe flow, the analytic solution is available. For turbulent pipe flow, the velocity field consists of average part and fluctuation part which plays an important role in the motion of particles because the characteristic length scale of the particles, i.e., the length of the particle, is much smaller than the turbulent Kolmogoroff length scale.

The fluctuation velocity field of fluid, $\boldsymbol{u}'$ is a Fourier series as follows (Wang and Stock, 1994; Fung et al., 1992):

$$\frac{\boldsymbol{u}'(\boldsymbol{x},t)}{\boldsymbol{u}_{rms}(\boldsymbol{x})}=\sum_{n=1}^{N}[(\boldsymbol{b}_n\times\boldsymbol{k}_n)\cos(\boldsymbol{k}_n\cdot\boldsymbol{x}-\omega_n t)+(\boldsymbol{c}_n\times\boldsymbol{k}_n)\sin(\boldsymbol{k}_n\cdot\boldsymbol{x}-\omega_n t)] \tag{6}$$

where, N is a large constant (N = 100 here), $\boldsymbol{b}_n$ and $\boldsymbol{c}_n$ are the vectors composed of Gaussian random numbers, frequency ω_n is also Gaussian random number, and wave number vector $\boldsymbol{k}_n$ is isotropic random vector on the surface of unit sphere. Therefore, the dot product of the coefficient of primary function and the wave number vector is zero ($(\boldsymbol{b}_n\times\boldsymbol{k}_n)\cdot\boldsymbol{k}_n=0$), which ensures the flow field incompressible.

In the computation, the diameter of pipe is 38 mm, and the mean flow velocities range from 0.18 to 3.7 cm s^{-1}. The average length of particles is 15 μm. In the computation, we have $50\leqslant Re\leqslant 10{,}000$, $0.1\leqslant\gamma\leqslant 6.8$ (γ is the shear rate of flow), $5\leqslant\boldsymbol{\beta}\leqslant 40$ and $2000\leqslant\boldsymbol{\rho}\leqslant 40{,}000$ (ρ is the particle density). 500 particles are initially distributed randomly at inlet. The density of particles is 2000 kg/m^3. The initial translational velocity and angular velocity for each particle are zero and the initial orientation vectors of particles are set isotropically on the surface of a unit sphere.

The numerical results show that in the laminar flow regime, more particles are aligned with the flow direction with increasing Re number. The shear rate of flow around a particle is the key factor for determining the orientation distribution of particles. The particle aspect ratio and particle density have insignificant influence (as shown in Fig. 4 where θ is the angle between the particle orientation and z axis), while particle velocity and particle St number have marginal influence, on the orientation distribution of particles. In the turbulent regime, the spatial and orientational distributions become more homogeneous with increasing Re number, which is consistent with the results given by Zhang et al. (2005). The fluctuation intensity of particle velocity in the streamwise direction is larger than that in the other two directions.

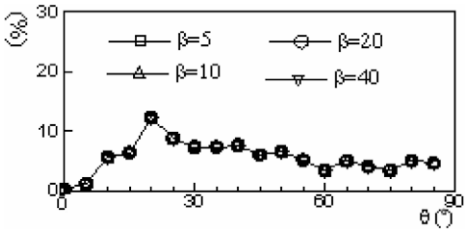

Fig. 4. Orientation distribution of particles with different aspect ratio β for Re = 100 and $St = 5.2\times10^{-5}$.

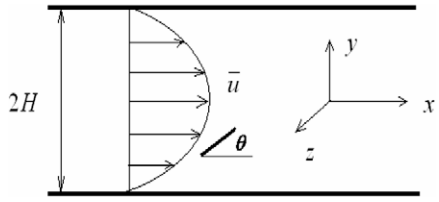

Fig. 5. Schematics of channel flow.

2.3. Channel flow

Turbulent channel flow is shown in Fig. 5. The research on the turbulent flow with the interaction between fluid and cylindrical particles is meaningful in the turbulent channel flow. Lin et al. (2006a) derived the modified Reynolds mean motion equation of turbulent cylindrical particulate flow and the equation of probability distribution function for mean particle orientation:

$$\frac{\partial\bar{u}_i}{\partial t}+\bar{u}_j\frac{\partial\bar{u}_i}{\partial x_j}=-\frac{1}{\rho}\frac{\partial\bar{p}}{\partial x_i}+\nu\frac{\partial^2\bar{u}_i}{\partial^2 x_j}-\frac{\partial\overline{u_i'u_j'}}{\partial x_j}+\frac{\mu_f}{\rho}\frac{\partial}{\partial x_j}\left(\overline{a_{ijkl}\varepsilon_{kl}}-\frac{1}{3}I_{ij}\overline{a_{kl}\varepsilon_{kl}}\right), \tag{7}$$

$$\frac{\partial\bar{\Psi}}{\partial t}+\bar{u}_j\frac{\partial\bar{\Psi}}{\partial x_j}-\bar{\omega}_{ji}p_i\frac{\partial\bar{\Psi}}{\partial p_j}+\lambda\overline{\varepsilon_{ji}}p_i\frac{\partial\bar{\Psi}}{\partial p_j}-\lambda\overline{\varepsilon_{kl}}p_k p_l p_j\frac{\partial\bar{\psi}}{\partial p_j}-\lambda\overline{\varepsilon_{kl}}\bar{\Psi}p_k p_l$$
$$=\alpha_{\Psi x}\frac{\partial^2\bar{\psi}}{\partial x_j^2}+\alpha_{\Psi p}\frac{\partial^2\bar{\psi}}{\partial p_j^2} \tag{8}$$

where u_i is the velocity, ρ is the pressure, ν is the kinematic viscosity of the fluid, μ_f is the apparent viscosity of the suspension, ε_{ij} is the tensor of strain rate, ψ is the probability distribution function for particle orientation, ω_{ij} is the vorticity tensor; p_i is a unit vector parallel to the particle's axis of symmetry, the parameter $\lambda=(\beta^2-1)/(\beta^2+1)$ (β is the aspect ratio of the particle), $\alpha_{\Psi x}$ and $\alpha_{\Psi p}$ are the dispersion coefficients of linear and angular displacements of the particles, respectively; "–" and " ′" represent mean and fluctuating quantities, a_{kl} and a_{ijkl} are the second- and fourth-orientation tensors of the cylindrical particles and defined by:

$$a_{ijkl}=\oint p_i p_j p_k p_l\psi(\boldsymbol{p})\mathrm{d}\boldsymbol{p}, \tag{9}$$

where $\boldsymbol{p}$ is a unit vector aligned along the particle's axis.

A new successive iteration method was developed to calculate the mean orientation distribution of particles and the mean and fluctuation-correlated quantities based on Eqs. (7), (8) in the turbulent channel flow. In the computation, the width of channel is 50 mm, the fluid is water with viscosity of 1.007×10^{-6} m^2/s, the particles are nylon with density of 1.04×103 kg/m^3, length of 20 μm and aspect ratio of 15. The Reynolds number and the particle mass concentration range from 1.1×104 and 2% to 2.5×104 and 5%, respectively. The results show that the flow rate of partic-

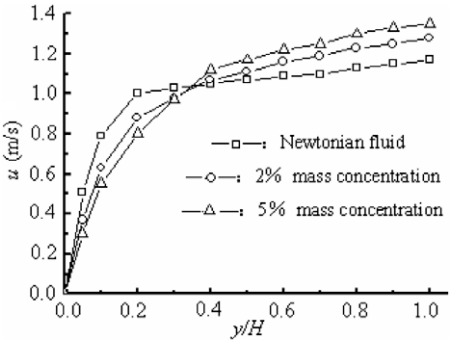

Fig. 6. Mean velocity for particulate flow with different concentration at $Re = 2.5\times104$, β = 15.

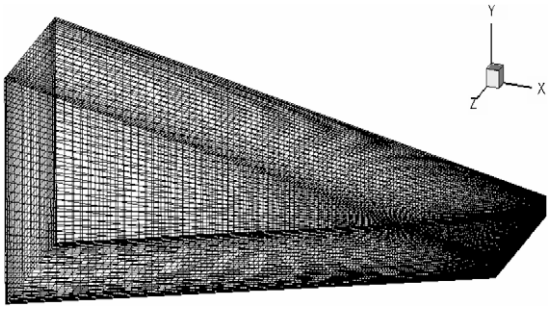

Fig. 7. Schematics of converging channel flow.

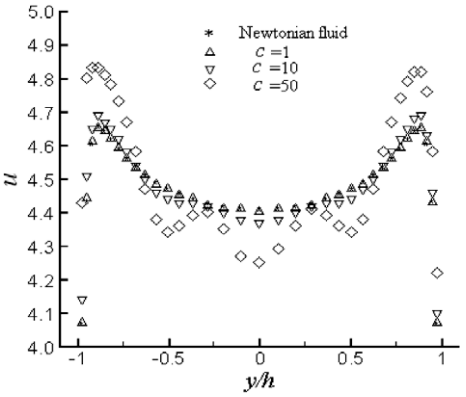

Fig. 8. Velocity profile at exit with different velocity augment ratio for $R = 11.2$, $\beta = 20$, $l = 1$ mm.

ulate flow is large under the same pressure drop in comparison with the rate of Newtonian fluid as shown in Fig. 6. Particles play a significant role in the drag reduction. The amount of drag reduction augments with increasing the particle mass concentration. The relative turbulent intensity and the Reynolds stress in the particulate flow are smaller than those in the Newtonian flow, which illustrates that the particles have an effect on suppressing the turbulence. The amount of suppression is directly proportional to the particle mass concentration.

2.4. Converging channel flow

The cylindrical particulate flow in a converging channel (Fig. 7) is involved in the pulp and paper industry where paper is formed from suspensions of cellulose particles. The properties of the final product usually depend on the velocity profile and the bulk stress. In order to understand the flow characteristics, it is important to know the effect of particles on the velocity profile, mean pressure, turbulent and rheological properties. Lin et al. (2004b) analyzed the pressure gradient force, Magnus force and Saffman force exerted on a moving cylindrical particle in a converging channel, and computed numerically these forces as well as the Stokes resistance, added mass and Basset force. The results show that the Stokes resistance, added mass and Basset force are much larger than the pressure gradient force, Magnus force and Saffman force. The effects of particle *St* number, particle initial orientation and flow flux on these forces are given.

Lin et al. (2007) solved the modified Reynolds mean motion Eq. (8) in the turbulent converging channel using the Reynolds stress model. A finite volume method was used in the solver. A velocity profile, turbulent intensity and characteristic scale were given as the inlet condition, and a pressure boundary condition was applied at exit. The no-slip condition for velocities was used on the wall. In the computation, the turbulent kinetic energy and the Kolmogoroff length scale were taken as 0.045 and 0.7 mm at inlet, respectively. The water with viscosity of $1.007 \times 10^{-6}\,m^2/s$ was taken as the suspending fluid. The particle length l and aspect ratio β are 1 mm and 20, respectively. The particle volumetric concentration $c = 1$, 10 and 50 ($c = nl^3$, where n is particle number density and l is particle half-length), respectively. The contraction ratio R is defined as the ratio of heights at inlet to that at exit. When suspension flows through the contraction, the streamwise mean velocity over the cross-section will augment along the flow direction because the cross section reduces and the flow is incompressible. The distributions of the mean velocity, mean pressure, turbulent kinetic energy and turbulent dissipation are obtained. It is found that, for higher particle concentration ($c = 50$), the mean velocities at exit are small in the regions near the center, while large near the wall (Fig. 8). Particles reduce turbulent intensity and turbulent dissipation at central line, but enhance them over the cross section at exit. Particles have no effect of restraint on the turbulence in the contraction flow. The additional stress resulting from particles plays a role in the increase of drag.

3. Sedimentation

The sedimenting behavior of cylindrical particles plays a critical role in many branches of science such as aerosol physics and atmospheric science. Available investigations have shown that non-spherical particles like cylinders will tend to exhibit preferential orientation while under going free fall through a quiescent fluid at intermediate *Re* numbers.

Lin et al. (2003b) used the lattice Boltzmann method to investigate the effects of particle aspect ratio on the sedimentation of single cylindrical particle in a Newtonian fluid. In the simulation, the computation box is moving with the particle. The diameter of the particle, D, is eight times of the lattice width. The terminal Reynolds number of particle is defined as $Re = (\alpha\rho\Delta\rho g d^3/2\mu^2 C_d)^{1/2}$ (ρ is the fluid density, $\Delta\rho$ is the density difference between the particle and the fluid, g is the gravity, d is the particle diameter, μ is the fluid viscosity, C_d is the drag coefficient). The particle aspect ratio ranges from 2 to 10. The results showed that the stable orientation of a single particle is the horizontal direction. The terminal *Re* number increases as the aspect ratio increases, and basically remains invariable when the aspect ratio is high enough as shown in Fig. 9 where the experiment results (Clift et al., 1978) are also given. The lateral drift of the particle is more apparent at higher aspect ratios and the orientation of the particle at which the lateral drifting velocity reaches the maximum is not sensitive to the value of the aspect ratio. When the aspect ratio is around 2.8, the particle rotates fastest from the vertical location to the hor-

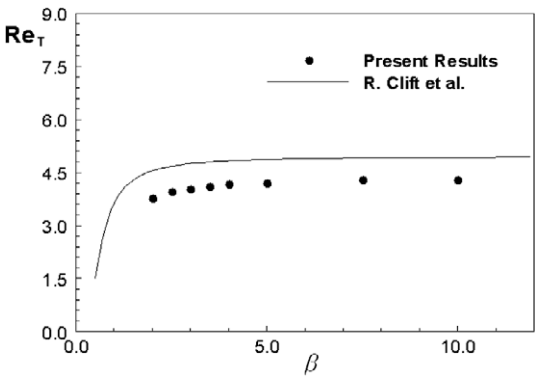

Fig. 9. Terminal *Re* number of particle vs. particle aspect ratio

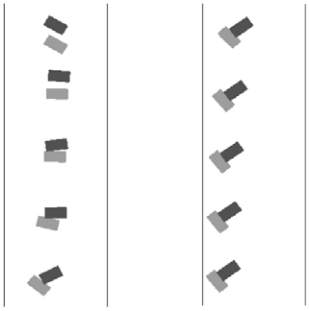

Fig. 10. Inverted T-structure.

izontal. Lin et al. (2004c) simulated numerically the sedimentations of cylindrical particles with three different initial relative positions using the lattice Boltzmann method. The results showed that, (i) if two particles are released parallel but separated horizontally, they push away each other, rotate inwards and separate horizontally as they fall; (ii) if two particles are released parallel but separated vertically, the sedimentation behavior can be classified into three stages: trailing, tumbling and separating; (iii) if two particles are released perpendicular but separated vertically, the sedimentation behavior can be characterized as: trailing and rotating, touching and sliding. In the sedimentation process, the particles rotate and drift at any initial orientation and terminal *Re* number. The orientation, lateral position, drift and sedimenting velocity of particles change periodically at small terminal *Re* number. With increasing terminal *Re* number, the periodicity disappears, and an inverted T-structure forms as shown in Fig. 10. This structure appears more quickly and lasts for a longer time at larger terminal *Re* number.

4. Structure feature and rheology property

4.1. Effective viscosity

Research on the dominant structural feature of cylindrical particulate suspensions is based on a statistical conception, i.e., the bulk quantity such as bulk stress is defined as averages over an ensemble of realizations. The contribution to the bulk quantity due to the presence of particles is expressed as integrals over the surfaces of particles. The orientation distribution function of particles and the integrals of it over the orientations, i.e. orientation tensors, can be used to describe the dynamical orientation state of the suspensions. Then the structural feature of the whole flows, such as the bulk stress and the bulk effective viscosity, can be determined. An important aspect in the mechanics of cylindrical particulate suspensions is to develop a suitable constitutive relation, by which the macroscopic rheological property of a suspension can be predicted from the orientations of particles.

The viscosity measurements have been performed by some researchers. However, the available expressions for the effective viscosity cannot provide good predictions compared with the experiment data measured in the semi-dilute shear flows of cylindrical particulate suspension with small aspect ratio. The departure of the theoretical prediction from the measured data increases with the decrease of the particle aspect ratio. Therefore, Zhang et al. (2004) performed an experiment to study the effective viscosity. In their experiment, the suspensions consist of glass in silicon oil with the viscosity of 0.474 Pa s and the density of 1 g/cm^3. The viscosity of the suspensions was measured by using a Hakke viscometer as shown in Fig. 11. The gap-to-particle-length ratio is higher than 7, so boundary effects are not significant for the measurements, and the produced shear flows are approximately uniform at the particle length scale. In the computation, we have $0.12 \leqslant c \leqslant 1.2$, $10 \leqslant \beta \leqslant 50$ and $0.01\ s^{-1} \leqslant \gamma \leqslant 100\ s^{-1}$. Based on experiment data, they proposed a new expression for the effective viscosity in the semi-dilute shear flows with small aspect ratio:

$$\bar{\mu}_e - 1 = \bar{\mu}_f \langle p_x^2 p_y^2 \rangle + C_V c^3, \tag{10}$$

where $\bar{u}_e$ is the effective viscosity, $\bar{u}_f$ is the additional viscosity due to the presence of particles, p_x and p_y are the components of the unit vector, $C_v = 900$ and c is the particle volumetric concentration. To prove the validity of Eq. (10), they compared the predicted data from Eq. (10) with the measured data of other investigators for various aspect ratios as shown in Fig. 12.

4.2. Turbulent channel flow

The rheological behavior of cylindrical particulate suspensions, mainly characterized by the shear stress and the first normal stress difference, in the turbulent channel flow as shown in Fig. 5 was studied by Lin et al. (2006b). The relationship between the shear stress σ_{12}, the first normal stress difference $\sigma_{11} - \sigma_{22}$ and the particle orientation tensors is given by (Dinh and Armstrong, 1984):

$$\sigma_{12} = \mu\dot{\gamma} + \mu_p a_{1122}\dot{\gamma}, \tag{11}$$

$$\sigma_{11} - \sigma_{22} = \mu_p(a_{1112} - a_{1222})\dot{\gamma}, \tag{12}$$

where μ is the viscosity of fluid; $\dot{\gamma}$ is the local mean shear rate of the turbulent flow; μ_p is the additional viscosity due to the presence of particles and given by $\mu_p = \pi\mu n L^3/6\ln(2\beta)$ (n is the particle number per unit volume; L is the particle length; β is the particle aspect ratio), a_{ijkl} is the fourth-order orientation tensors defined by Eq. (9) in which ψ is the orientation distribution function of particles, and is given by (Advani and Tucker (1987)):

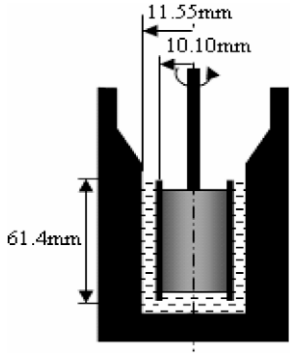

Fig. 11. The sketch map of Hakke viscometer

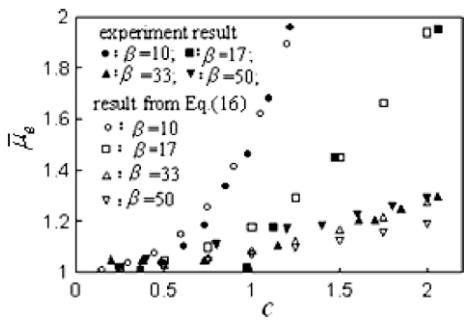

Fig. 12. Effective viscosity vs. particle concentration.

$$\frac{\partial \psi}{\partial t} + \nabla_p \cdot (\dot{p}\psi) = 0, \tag{13}$$

Dividing ψ and $\dot{\boldsymbol{p}}$ into mean and fluctuating parts, then substituting into Eq. (13), we can obtain the equation for $\bar{P}si$ at a steady state:

$$\frac{1}{\sin\theta}\frac{\partial\left(\sin\theta\cdot\bar{\dot{\theta}}\bar{\psi}\right)}{\partial\theta} + \frac{\partial(\bar{\dot{\varphi}}\bar{\psi})}{\partial\varphi} = \frac{1}{\sin\theta}\frac{\partial}{\partial\theta}\left(\sin\theta\cdot D_\theta\frac{\partial\bar{\Psi}}{\partial\theta}\right) + \frac{\partial(J_\varphi)}{\partial\varphi} \tag{14}$$

where D_θ and j_φ are the orientation dispersion coefficients along θ and ϕ as shown in Fig. 13 (the expressions of D_θ and j_φ are complex and can be found in the reference (Lin et al. 2006b). Eq. (14) was numerically solved to obtain $\bar{P}si$ by using the finite differential method. For the convenience of the simulation, Eq. (14) was replaced by its unsteady version. The scheme of time advance adopted the fourth-order Rung–Kutta method. The convection terms were discretized by using the upwind difference scheme, while the diffusion terms using the central difference scheme. Then the shear stress and first normal stress difference were calculated based on Eqs. (10)–(12). In the computation, the width of channel is 50 mm, the fluid is water with viscosity of 1.007×10^{-6} m^2/s, the particle volumetric concentration $c = 0.667\%$ ($c = \alpha nLLd^2/4$). The Reynolds number ranges from 2500 to 11,000. The results show that the shear stress increases, while the first normal stress difference decreases, as shown in Fig. 14, from the wall to the center of the flow for varying *Re* number.

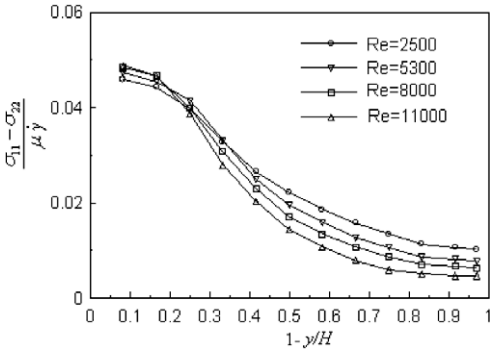

Fig. 14. Distribution of first normal stress difference for $c = 0.667\%$.

5. Hydrodynamic instability

5.1. Channel flow

The mode of hydrodynamic instability is responsible for the evolution of the flow, it is significant to understand the effects of particle on the instability. However, very limited attention has been devoted to the instability of cylindrical particulate suspensions.

You et al. (2004) performed a linear stability analysis for the cylindrical particulate suspensions in a channel flow as shown in Fig. 5. Based on the slender-body theory, they derived a modified stability equation:

$$\begin{aligned} &i\alpha[(U_0-c)(D^2-\alpha 2)-D^2U_0]\varphi' - \frac{1}{Re}(D^2-\alpha^2)^2\varphi' \\ &\quad = H[(D^2+\alpha^2)F_{12} + i\alpha D(F_{11}-F_{22})], \end{aligned} \tag{15}$$

where α is the wavenumber; U_0 is streamwise velocity in base-state; $c = c_r + ic_i$ (c_i is the growth rate of the perturbation, c_r is the propagation velocity of perturbation); $D = \mathrm{d}/\mathrm{d}y$; *Re* is the Reynolds number; φ' is the amplitude of small perturbation for streamfunction; H is the ratio between the axial stretching resistance of particles and the inertial force of the fluid; F_{ij} is the product of the fourth-order particle orientation tensor and the rate of the fluid strain tensor. The natural closure approximation, as shown in Eq. (15), was used to determine the particle orientation.

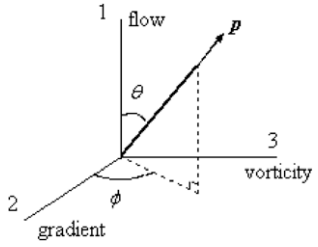

Fig. 13. Effective viscosity vs. particle concentration.

$$a_{ijkl} = \frac{det(a_{ij})}{6}(\delta_{ij}\delta_{kl}+\delta_{ik}\delta_{jl}+\delta_{il}\delta_{jk}) + \frac{1}{3}(a_{ij}a_{kl}+a_{ik}a_{jl}+a_{il}a_{jk}) \tag{16}$$

where a_{kl} and a_{ijkl} are the second- and fourth-orientation tensors of the particles and defined by Eq. (9). The ordinary differential equations were replaced by a set of finite difference equations and then transformed into a group of algebraic equations. For arbitrary given real values of *Re*, α and H, the algebra equations were solved using iterative method to find the complex eigenvalues c.

In the computation, the orientational diffusivity coefficient, C_I, that accounts for the inter-fiber hydrodynamic interactions are within 10^{-3} to 10^{-2}. The Reynolds number ranges from 5000 to 30,000. It is found that the flow instability is governed by H and C_I. The increment of H or C_I causes an increase of critical *Re* number (Fig. 15), a reduction of the maximum perturbation growth rate (Fig. 16). Hence, the particles effectively attenuate the instability of the flow, and this effect is clearer for higher values of *Re* number.

5.2. Taylor–Couette flow

Wan and Lin (2004) performed a linear stability analysis of the Taylor–Couette flow between two rotating coaxial cylinders, as shown in Fig. 17, in the presence of semi-concentrated cylindrical particles. They derived a modified stability equations:

$$\begin{aligned} &\left[(\mathrm{DD}_*-\alpha^2-\lambda)(\mathrm{DD}_*-\alpha^2)+H'\frac{\alpha^2}{r^2}\right]u \\ &\quad = \frac{2\alpha^2 Re_1 V_0}{r}v;\ (\mathrm{DD}_*-\alpha^2-\lambda)v = Re_1(D_*V_0)u, \end{aligned} \tag{17}$$

where $D^* = d/dr+1/r; D = d/dr$; α is the wave number along the axial direction; λ is the growth rate of the perturbation; H′ is the param-

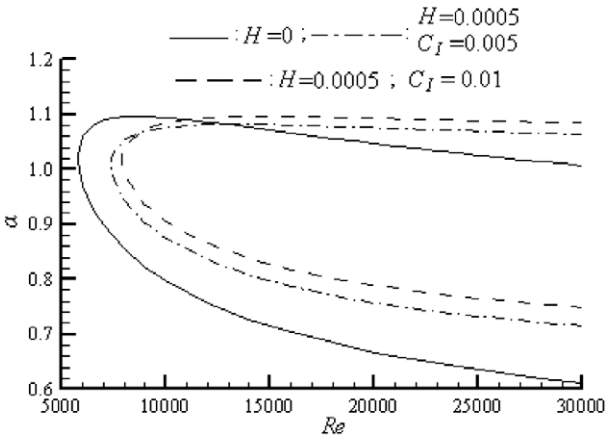

Fig. 15. Neutral instability curves

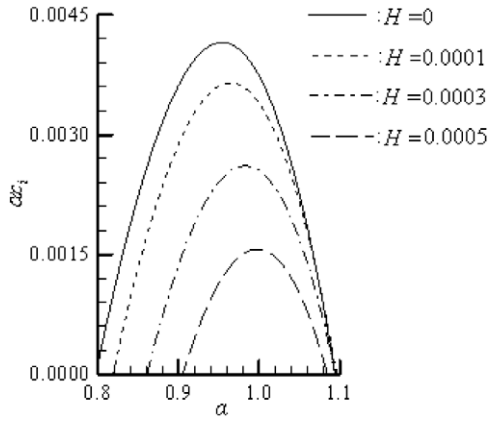

Fig. 16. Growth rate of perturbation as a function of the wavenumber (Re = 10,000, C_I = 0.01)

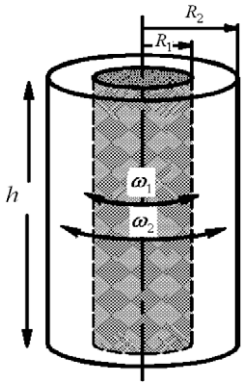

Fig. 17. Schematic of Taylor–Couette flow.

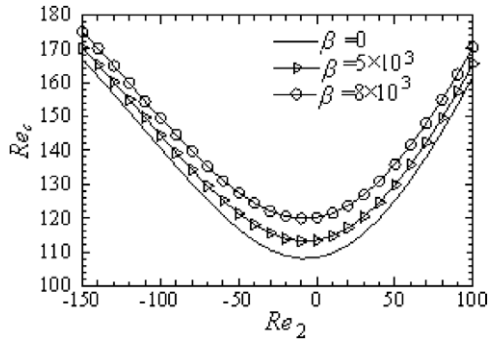

Fig. 18. Stability regions at different aspect ratio β.

eter related to the particle aspect ratio β and the particle volumetric concentration c; r is the radial coordinate; $Re_1 = \omega_1 R_1 \delta/\nu$ (ω_1 and R_1 are the angular velocity and radius of the inner cylinder, respectively, $\delta = R_2 - R_1$, ν is the viscosity of the fluid); V_0 is the circumferential velocity in base-state; u and v are the amplitude of small perturbation for velocities along radial and circumferential direction, respectively. The solution to the eigenvalue problem for Eq. (16) is obtained numerically by using the finite difference method. In the computation, the particle volumetric concentration and the radius ratio of two cylinders $\eta = R_1/R_2$ range from 0 and 0.8 to 0.5×10^{-4} and 0.975, respectively. The results show that the particles have a stabilizing effect on the flow, and this effect is more obvious for the cases with higher particle volumetric fraction c, larger particle aspect ratio β as shown in Fig. 18 (where $Re_2 = \omega 2R2\delta/\nu$ with ω_2 and R_2 being the angular velocity and radius of the outer cylinder, respectively), and lower radius ratio of two cylinders η.

Acknowledgement

This research was supported by the Major Program of the Scientific Project of Zhejiang Province of China with Grant No. 2008C01024-4.

References

Advani, S.G., Tucker, C.L., 1987. The use of tensors to describe and predict fiber orientation in short fiber composites. J. Rheol. 31, 751–784.
Batchelor, G.K., 1970. Slender-body theory for particles of arbitrary cross-section in Stokes flow. J. Fluid Mech. 44, 419–440.
Clift, R., Grace, R.J., Weber, M.E., 1978. Bubble Drops and Particles. Academic Press, New York.
Dinh, S.M., Armstrong, R.C., 1984. A rheological equation of state for semi-concentrated Fiber suspension. J. Rheol. 28, 207–227.
Fung, J.C.H., Hunt, J.C.R., Malik, N.A., Perkins, R.J., 1992. Kinematic simulation of homogeneous turbulence by unsteady random Flourier modes. J. Fluid Mech. 236, 281–318.
Lin, J.Z., Gao, Z.Y., Zhou, K., Chan, T.L., 2006a. Mathematical modeling of turbulent fiber suspension and successive iteration solution in the channel flow. Appl. Math. Model. 30, 1010–1020.
Lin, J.Z., Li, J., Zhang, W.F., 2004b. The force for cylindrical particles in an elongational-shear flow. J. Nonlinear Sci. Numer. Simul. 5, 9–16.
Lin, J.Z., Shao, X.M., Shi, X., Yu, Z.S., 2004c. Study on the interaction of sedimenting cylindrical particles in still fluid. Acta Mech. Sin. 20, 33–45.
Lin, J.Z., Shi, X., You, Z.J., 2003b. Effects of the aspect ratio on the sedimentation of a fiber in Newtonian fluids. J. Aerosol Sci. 34, 909–921.
Lin, J.Z., Shi, X., Yu, Z.S., 2003a. The motion of cylindrical particles in an evolving mixing layer. Int. J. Multiphase Flow 29, 1355–1372.
Lin, J.Z., Zhang, L.X., Zhang, W.F., 2006b. Rheological behavior of fiber suspensions in a turbulent channel flow. J. Colloid Interface Sci. 296, 721–728.
Lin, J.Z., Zhang, S.L., Olson, J.A., 2007. Effect of fibers on the flow property of turbulent fiber suspensions in a contraction. Fibers Polym. 18, 60–65.
Lin, J.Z., Zhang, W.F., Yu, Z.S., 2004a. Numerical research on the orientation distribution of fibers immersed in laminar and turbulent pipe flows. J. Aerosol Sci. 35, 63–82.
Mackaplow, M.B., Shaqfeh, E.S.G., 1998. A numerical study of the sedimentation of fiber suspension. J. Fluid Mech. 376, 149–182.
Wan, Z.H., Lin, J.Z., 2004. Hydrodynamic instability of semi-concentration fiber suspensions between two rotating coaxial cylinders. Int. J. Nonlinear Sci. Numer. Simul. l.5, 211–216.
Wang, L.P., Stock, D.E., 1994. Numerical simulation of heavy particle dispersion-scale ratio and flow decay considerations. ASME J. Fluid Eng. 116, 154–163.
You, Z.J., Lin, J.Z., Yu, Z.S., 2004. Hydrodynamic instability of fibre suspensions in channel flows. Fluid Dyn. Res. 34, 251–271.
Zhang, L.X., Lin, J.Z., Shi, X., 2004. Modified expression for the effective viscosity in the semi-dilute shear flows of fiber suspension. Chin. Sci. Bull. 49, 1453–1456.
Zhang, L.X., Lin, J.Z., Chan, T.L., 2005. Orientation distribution of cylindrical particles suspended in a turbulent pipe flow. Phys. Fluids 17, 1–8.